On using enriched cover function in the partition-of-unity method for singular boundary-value problems

Fan, S. C.; Liu, X.; Lee, Chi King

2002

Liu, X., Lee, C. K., & Fan, S. C. (2002). On using enriched cover function in the Partition-of-unity method for singular boundary-value problems. Computational Mechanics, 29(3), 212-225.

https://hdl.handle.net/10356/103089

https://doi.org/10.1007/s00466-002-0335-x

On using enriched cover function in the Partition-of-unity method for singular boundary-value problems

[1]X Liu, [2]C K Lee, [3*]S C Fan

School of Civil and Environmental Engineering,
Nanyang Technological University, Nanyang Avenue, Singapore 639798

E-mails: [1]cxliu@ntu.edu.sg, [2]ccklee@ntu.edu.sg, [3]cfansc@ntu.edu.sg,

Pre-print for the paper in

Computational Mechanics 29 (2002) 212–225 _ Springer-Verlag 2002

Number of pages: 29

Number of figures: 24

Number of Tables: 12

*Correspondence author

ABSTRACT Amongst the various approaches of 'meshless' method, the Partition-of-unity concept married with the traditional finite-element method, namely *PUFEM*, has emerged to be competitive in solving the boundary-value problems. It inherits most of the advantages from both techniques except that the beauty of being 'meshless' vanishes. This paper presents an alternative approach to solve singular boundary-value problems. It follows the basic *PUFEM* procedures. The salient feature is to enhance the quality of the influence functions, either over one single nodal cover or multi-nodal-covers. In the vicinity of the singularity, available asymptotic analytical solution is employed to enrich the influence function. The beauty of present approach is that it facilitates easy replacement of the influence functions. In other words, it favors the 'influence-function refinement' procedure in a bid to search for more accurate solutions. It is analogous to the '*p*-version refinement' in the traditional finite-element procedures. The present approach can yield very accurate solution without adopting refined meshes. As a result, the quantities around the singularity can be evaluated directly once the nodal values are solved. No additional post-processing is needed. Firstly, the formulation of the present *PUFEM* approach is described. Subsequently, illustrative examples show the application to three classical singular benchmark problems having various orders of singularity. Results obtained through mesh refinements, single-nodal-cover refinements or multi-nodal-cover refinements are compared.

1

Introduction

Recently, the development of the so-called ‘meshless’ methods has attracted the attention of researchers endeavoring in the advancement of numerical technology. Various formulations or approaches have been reported. The word ‘meshless’ was never used in the earlier developments. Tracing the literature could find a seemingly earliest report (1977) by Lucy [1], who named it the ‘Smoothed Particle Hydrodynamics’ method. In the nineties, various approaches blossom out to be competitive. Still, they bear different names. Nayroles et al [2] called their method the ‘Diffuse element method’; Belytschko et al [3-4] called theirs ‘Element-free Galerkin method’; Liu et al [5] named theirs the ‘Reproducing kernel particle method’; Oden, Duarte and Zienkiwicz [6-7] called theirs figuratively the ‘HP-clouds method’; Babuska and Melenk presented it in the name of ‘Partition of unity finite element method’ [8-9] and Strouboulis et al [10] called his the ‘Generalized finite element method’ (though these are not really meshless); Onate et al [11] named his the ‘Finite point method’; Shi [12] called his the ‘Numerical manifold method’; and Braun et al. [13] just called it ‘Natural Element Method’. Lately amongst others, Atluri et al [14] presented his truly meshless method using the local Moving-Least-Square Petrov-Galerkin approach. Essentially, the shape functions in almost all these approaches could satisfy the partition-of-unity condition [15]. It is simple as it is named. For a given physical problem, the representative value and/or its derivatives at a finite number of nodes (or points) are chosen as the unknowns to be solved. The nodes are arbitrarily spaced. Each node has assigned a set of prescribed influence functions, which is defined over its neighboring domain. At any location among the nodes, the total influence derived from all nodes is normalized to unity. In other words, the influence to that particular location by any single node constitutes a certain percentage. The differences among the various approaches lie in the choice of the prescribed

influence functions and the ways of partitioning. Apparently, most approaches use a kind of continuous smooth weight function to describe the manner of partitioning. However, difficulties are encountered when it is employed to solve boundary-value problems. Attempts have been made to overcome or circumvent these difficulties. The often-used techniques are the collocation method, Lagrange multiplier, constraint equations or penalty method - to name a few. An alternative simple technique is to marry the partition-of unity concept with the well-developed finite-element method, namely *PUFEM*. The interpolation functions within an element, namely shape functions, are chosen as the partition-of-unity functions. As such, the difficulties in imposing the essential boundary conditions are alleviated [16]. On one hand, it inherits the advantages of the partition-of-unity concept but on the other hand, the beauty of being 'meshless' vanishes. In a bid to search for more accurate solutions, the same extent of pains will be experienced as in the traditional finite element analysis, in particular for a singular problem. It demands progressively finer meshes. Although some automatic adaptive re-meshing techniques have been developed to alleviate the pain [17-18], still the efficiency depends on their error-estimation and mesh-refinement algorithms. Very often, the computational cost is compromised. Other approaches of dealing with the singular problems are reported, such as those uniquely defined elements or intricate super-elements with incorporated singular function [19-21]. Reportedly, their performance is not fully satisfactory. On the other hand, Belytschko et al [3, 22] and Babuska et al [23] reported successful development of adding singular functions to a partition-of-unity.

This paper presents an alternative approach to solve singular boundary-value problems. It follows the basic *PUFEM* procedures. The salient feature is to enhance the quality of the nodal cover function, which comprises the nodal influence functions. In the vicinity of the singularity, the influence function adopts the available asymptotic analytical solutions. The beauty of present approach is that it facilitates easy replacement of the influence functions. In

other words, it favors the 'influence-function refinement' procedure in a bid to search for more accurate solutions. It is analogous to the '*p*-version refinement' in the traditional finite-element procedures. Contrary to the mesh-refinement approach, which is sometimes called the '*h*-version' refinement, the present approach can yield very accurate solution without employing a refined mesh. As a result, the quantities around the singularity can be evaluated directly once the nodal values are solved. No additional post-processing is needed.

Next section will present the formulation of the present *PUFEM* approach. Subsequently, illustrative examples show the application to three classical singular benchmark problems having various orders of singularity. Results obtained through mesh refinements, single-nodal-influence-function refinements or multi-nodal-influence-function refinements are compared. The accuracy and convergence of the present approach are analyzed.

2

Formulation of PUFEM with enriched cover functions

As mentioned above, various approaches of 'meshless' method are essentially either implicit or explicit form of the Partition-of-unity method (*PUM*). In fact, the traditional finite-element method (*FEM*) can be viewed as a special form of the *PUM*. In both *PUM* and *FEM*, the representative value and/or its derivatives at a finite number (n) of nodes (or points) are chosen as the unknowns to be solved. The nodes are also arbitrarily spaced. The differences lie in the definition of approximation in the form of interpolation or influence function.

2.1

Approximation functions

In the *FEM*, the domain $\boldsymbol{\Omega}$ of the physical problem is divided into a finite number of non-overlapping sub-domains $\boldsymbol{\Omega}_i$. The quantities at position $\boldsymbol{x}$ within each sub-domain is defined by local interpolation function $\boldsymbol{u}^e(\boldsymbol{x})$ between the n^e vertices/nodes of that element as follows:

$$\boldsymbol{u}^{e}(\mathbf{x}) = \sum_{j=1}^{n^{e}} \boldsymbol{N}_{j}(\mathbf{x})\, \mathbf{u}^{\mathbf{e}}(\mathbf{x}_{j}) \tag{1}$$

in which $\boldsymbol{x}_j$ denotes the coordinates vector at the node j and $\boldsymbol{N_j(x)}$ denotes the shape function associated with node j.

The distinct difference between the *FEM* and the *PUM* lies in the manner of partitioning. In the general *PUM*, all nodes, be it near or far, participated **directly** to the total sum (=unity) at an arbitrary location. Peculiar to others, the *PUFEM* limits the extent of participation only from nodes of the element where the interested point locates. In the context of *PUFEM*, the shape function $\boldsymbol{N_i(x)}$ is in fact a kind of *PU* function $\boldsymbol{\varphi_j(x)}$, which defines the percentage participation of the node i in that particular location. Besides, the *PUM* distinguishes itself from the *FEM* by having a set of prescribed nodal influence functions $\boldsymbol{\psi_{ij}(x)}$ for each node i. The quantities at an arbitrary location is now obtained by the global interpolation function $\boldsymbol{u}(\boldsymbol{x})$ as follows:

$$\boldsymbol{u}(\mathbf{x}) = \sum_{i=1}^{n} \varphi_{\boldsymbol{i}}(\mathbf{x}) \sum_{j=1}^{m_i} a_{ij} \psi_{\boldsymbol{ij}}(\mathbf{x}) \tag{2}$$

where a_{ij} denotes the generalized nodal values, m_i denotes the number of terms of the influence function employed at node i, and $\mathbf{x}$ denotes the coordinates vector $\mathbf{x}(x,y)$. It is worth noting that the *FEM* can be viewed as having influence function equal to one for all nodes.

2.2

Partition-of-unity functions

In the *PUFEM*, the *PU* function is not defined over a sub-domain comprising only a single element. Instead, it is defined over a group of neighboring elements, namely a *cover*. In mathematics, it can be described as follows. In an n-dimensional bounded domain $\boldsymbol{\Omega} \subset \Re^N$ ($N=1,2,3$), it consists of a set of open covers $\boldsymbol{\Omega_i}$ ($i=1,2, \ldots n$). Within each $\boldsymbol{\Omega_i}$, there is a node

x_i, which is not necessary at the center. The *PU* functions φ_i associated with a cover Ω_i satisfy the following conditions:

$$0 \le \varphi_i(x) \le 1 \qquad \forall x \in \Re^N \tag{3a}$$

$$\sum_{i=1}^{n} \varphi_i(x) = 1 \qquad \forall x \in \Omega \tag{3b}$$

There are many ways to construct the *PU* functions. For example, the linear vertex shape function in *FEM* is identical to the C^0 *PU* function; B_3-spline [24] can be employed to construct the C^2 *PU* function, etc. In this study, the C^0 *PU* functions are used (see Fig.1a).

2.3

Shape of cover

In the general *PUM* formulation, the cover of a node can be any convenient shape. It could be circular, elliptical, rectangular or polygonal, and is not necessary to be convex. However, in the *PUFEM* formulation, the cover of a node comprises a patch of elements surrounding and connected to that node (see Fig.1b). The shape depends on the finite element mesh. For example (see Fig.1b), the cover of node 1 is the polygonal region (Ω_1) bounded by the vertices *2-3-4-9-7-2*; the cover of node 9 is the polygonal region (Ω_9) bounded by the vertices *7-1-4-5-10-7*; similarly the cover of node 7 is the polygonal region (Ω_7) bounded by the vertices 7:8-*2-1-9-10-8*. At any location within the common triangular region $\Omega_1 \cap \Omega_9 \cap \Omega_7$, the summation of all participating *PU* functional values $[\varphi_1(x)+\varphi_9(x)+\varphi_7(x)]$ is equal to unity. With the same procedure, quadrangle element can be formed. In addition, elements are also used as integration cells in the following calculations.

2.4

Cover functions and enriched cover functions

For an arbitrary nodal cover Ω_i, the general form of nodal cover function is a linear combination of its nodal influence functions $\psi_{ij}(x)$ as follows:

$$\boldsymbol{F}_i(\mathbf{x}) = \sum_{j=1}^{m_i} a_{ij}\, \boldsymbol{\psi}_{ij}(\mathbf{x}) \tag{4}$$

The coefficients a_{ij} are regarded as the generalized nodal values. The influence function $\boldsymbol{\psi_{ij}(x)}$ may adopt polynomial basis functions or any other analytical basis functions. It is worth noting that different influence or cover functions could be employed for different covers. In general, polynomial basis functions are used. Analytical basis functions are usually employed only in the near region of a singularity. Hence, this formulation facilitates easy replacement of cover functions. In other words, it favors the 'influence-function refinement' procedure in a bid to search for more accurate solutions. It is analogous to the '*p*-version refinement' in the traditional finite-element procedures. It can yield very accurate solution without employing a refined mesh. The refinement is achieved either by employing higher order polynomial-basis influence functions or by using available asymptotic analytical functions. A cover function, which comprises the asymptotic influence functions, is called *enriched cover functions*. What follows give the explicit forms of the first ($p=1$) to fourth ($p=4$) ordered polynomial basis influence functions.

- 1^{st} order ($p=1$) polynomial basis influence function having one term ($m_i=1$) for node i:

$$\boldsymbol{\Psi}_{i1} = 1 \tag{5}$$

- 2^{nd} order ($p=2$) polynomial basis influence function having 3 terms ($m_i=3$) for node i:

$$\boldsymbol{\Psi}_{i1} = 1\ ; \qquad \boldsymbol{\Psi}_{i2} = (x - x_i)^2\ ; \quad \boldsymbol{\Psi}_{i3} = (y - y_i)^2 \tag{6a-c}$$

- 3^{rd} order ($p=3$) polynomial basis influence function having 7 terms ($m_i=7$) for node i:

$$\boldsymbol{\Psi}_{i1} = 1\ ; \qquad \boldsymbol{\Psi}_{i2} = (x - x_i)^2\ ; \quad \boldsymbol{\Psi}_{i3} = (y - y_i)^2 \tag{7a-c}$$

$$\boldsymbol{\Psi}_{i4} = (x - x_i)^3\ ; \qquad \boldsymbol{\Psi}_{i5} = = (x - x_i)^2 (y - y_i) \tag{7d-e}$$

$$\boldsymbol{\Psi}_{i6} = (x - x_i)(y - y_i)^2\ ; \qquad \boldsymbol{\Psi}_{i7} = (y - y_i)^3 \tag{7f-g}$$

- 4^{th} order ($p=4$) polynomial basis influence function having 12 terms ($m_i=12$) for node i:

$$\boldsymbol{\Psi}_{i1} = 1\ ; \qquad \boldsymbol{\Psi}_{i2} = (x - x_i)^2\ ; \quad \boldsymbol{\Psi}_{i3} = (y - y_i)^2 \tag{8a-c}$$

$\Psi_{i4} = (x - x_i)^3$; $\Psi_{i5} = = (x - x_i)^2 (y - y_i)$ (8d-e)

$\Psi_{i6} = (x - x_i)(y - y_i)^2$; $\Psi_{i7} = (y - y_i)^3$ (8f-g)

$\Psi_{i8} = (x - x_i)^4$; $\Psi_{i9} = = (x - x_i)^3 (y - y_i)$ (8h-i)

$\Psi_{i10} = (x - x_i)^2 (y - y_i)^2$; $\Psi_{i11} = (x - x_i)(y - y_i)^3$ (8j-k)

$\Psi_{i12} = (y - y_i)^4$ (8n)

It is worth noting that the linear terms *x*, *y* and *xy* are excluded from the above lists of influence functions. It is because they lead to linear dependency in the interpolation function $\boldsymbol{u}(\boldsymbol{x})$. Reference [7] gives the detailed explanation.

In the near region of a singularity, enriched nodal cover functions are favored. Note that adoption of enriched cover functions is not limited to a single node where lies the singularity. A cluster of nodes in the vicinity of singularity may employ the same form of enriched cover functions. For an arbitrary node *k*, asymptotic form of influence function $\psi(r,\theta) = r^{\beta} f(\theta)$ is used to replace the general form (Eq. 4), and the cover function can be expressed as follows.

$$F_k(r,\theta) = a_{k1} + \sum_{j=2}^{m_k^e} a_{kj} r^{\beta_j} f_{kj}(\theta) \tag{9}$$

which is expressed in terms of the polar coordinates (r, θ) having the pole ($0,0$) located at the singular point. The coefficient *'β'* lies in the range: $1>\beta>0$, and $f_{kj}(\theta)$ is an available analytical solution in terms of θ. The enriched cover function comprises m^e_k terms. Note that the first enriched basis function equals to 1 (i.e. $\Psi_{k1}=1$), and the associated coefficient a_{k1} represents the rigid-body movement. When only one term is employed ($m^e_k=1$), it is identical to the general polynomial-typed cover function for $m_k=1$.

2.5

Single and multi-nodal cover enrichment schemes

The present formulation offers options of single or multi-nodal cover enrichment schemes, shortly termed ‘single enrichment’ and ‘multi-enrichment’ respectively. If 'single enrichment’ is opted, the obvious choice is to have the cover functions of the singularity node enriched. When ‘multi-enrichment’ is opted, enriched cover functions are adopted for a cluster of nodes in the vicinity of the singularity node. Figure 2a shows the enriched domain arising from a single enrichment, and Figure 2b shows the enriched domain arising from an arbitrary 3-nodal enrichment scheme.

During the numerical evaluation, sequence of computations goes from one sub-domain to another, or element by element. Hence, it is more convenient to re-write the approximation function $\boldsymbol{u}(x)$ for each sub-domain according to the element boundaries. As mentioned earlier, the shape function $\boldsymbol{N_i(x)}$ used in the standard *FEM* is in fact a kind of C^0 *PU* function. In this study, $\boldsymbol{\varphi_i(x)}$ is set equal to $\boldsymbol{N_i(x)}$. Hence, substituting $\boldsymbol{\varphi_i(x)=N_i(x)}$ into Eq. (2) yields the form ready for sub-domain computations. For example, a quadrilateral element having four corner nodes (1, 2, 3 and 4) and not falling into any enriched domain would have an approximation function of the following form:

$$\boldsymbol{u}(\mathbf{x}) = \sum_{i=1}^{4} \boldsymbol{N}_i(\mathbf{x}) \left[\sum_{j=1}^{m_i} a_{ij}\, \boldsymbol{\psi}_{ij}(\mathbf{x}) \right] \tag{10}$$

in which $\boldsymbol{\psi}_{ij}$’s are polynomial-typed influence functions. If the element falls into an enriched domain, which happens to be the overlapping region of two enriched covers (e.g. nodes 1 and 4), the approximation function becomes the following form:

$$\begin{aligned} \boldsymbol{u}(\mathbf{x}) = {} & \boldsymbol{N}_1(\mathbf{x}) \overbrace{\left[a_{11} + \sum_{j=2}^{m_1^e} a_{1j} r^{\beta_j} f_{1j}(\theta)) \right]}^{enriched\ \ cover\ \ function} + \sum_{i=2}^{3} \boldsymbol{N}_i(\mathbf{x}) \overbrace{\left[\sum_{j=1}^{m_i} a_{ij} \psi_{ij}(\mathbf{x}) \right]}^{polynomial\ \ cover\ \ functions} \\ & + \boldsymbol{N}_4(\mathbf{x}) \overbrace{\left[a_{41} + \sum_{j=2}^{m_4^e} a_{4j} r^{\beta_j} f_{4j}(\theta)) \right]}^{enriched\ \ cover\ \ function} \end{aligned} \tag{11}$$

Note that in general, the numbers of terms of nodal influence function employed at different nodes, (be it enriched or not), are not necessarily the same, i.e. $m^e_{1\neq}\, m_{2\neq}\, m_{3\neq}\, m^e_4$.

3

Numerical Examples

In this section, several singular problems are solved using the *PUFEM*. Formation of algebraic equations is similar to those in the standard *FEM* procedures. During the numerical evaluation, computations are carried out element by element. Gauss quadrature is used for numerical integration. In general, *5×5* Gauss points are used when 1^{st} or 2^{nd} (*p=1* or *2*) ordered polynomial influence functions are in place; *10×10* Gauss points are used for *p=3* or 4; and *20x20* Gauss points are used for *p=5*. In each example, the performance of single versus multi-enrichment scheme is investigated. In addition, the improvements through the employment of higher-order polynomials or asymptotic functions are studied. The performance is also compared with those results obtained through mesh refinement (*h*-refinement).

3.1

Example 1: Laplace equation defined over an L-shaped domain

The Laplace equation defined over an *L*-shaped domain shown in Fig.3 is taken as the first example. The governing differential equation and boundary conditions for this problem are:

$$\begin{cases} -\Delta u = 0 & on \quad \Omega \\ u = 1 & on \quad x = -1, -1 \le y \le 1 \\ u = 0 & on \quad x = 1, -1 \le y \le 0 \\ \dfrac{\partial u}{\partial n} = 0 & on \quad all \quad other \quad boundaries \end{cases} \tag{12}$$

The singular point locates at A ($r=0$), where the first derivative of the exact solution $\boldsymbol{u_{ex}'}$ is unbounded and of the order $r^{-1/3}$. The exact solution $\boldsymbol{u_{ex}}$ in the vicinity of the singular point A has the following form [21]:

$$\boldsymbol{u}_{ex} = \sum_{n=0}^{2} C_n r^{2n/3} \cos[(2n/3)\theta], \qquad -\frac{3}{2}\pi \le \theta \le 0 \tag{13a}$$

where $C_0 = 0.6667$, $C_1 = -0.4520$, $C_2 = -0.2149$ (13b)

Hence, the asymptotic influence functions may adopt the following forms:

$$\boldsymbol{\psi}_{i1} = 1 \quad , \quad \boldsymbol{\psi}_{i2} = r^{2/3}\cos(\frac{2\theta}{3}) \tag{14a-b}$$

$$\boldsymbol{\psi}_{i3} = r^{4/3}\cos(\frac{4\theta}{3}) \quad , \quad \boldsymbol{\psi}_{i4} = r^2\cos(2\theta) \tag{14c-d}$$

The performance of single versus multi-enrichment scheme is investigated. Under the single-enrichment scheme, only the cover function for the re-entrant corner node A is enriched (see Figs. 4a, 5a and 6a). The enriched domain is a small region surrounding the singular node A. Under the multi-enrichment scheme, a cluster of nodal covers (including the node A's) is enriched (see Figs. 4b, 5b and 6b). It results in an enlarged enriched domain covering at least a quarter of the whole problem domain. In both schemes, various results are obtained through p-refinements using one, two, three or four terms ($m^e=1$ *to* 4) of enriched functions for the enriched covers. On the other hand, the effects of h-refinements are also investigated through employment of 3 different meshes. Mesh-I has *21* nodes and *12* elements (see Figs. 4a and 4b). All elements have the same size (*0.5x0.5*). Mesh-II has *65* nodes and *48* elements (see Figs. 5a and 5b). All elements have the same size (*0.25x0.25*). Mesh-III has *225* nodes and *192* elements (see Figs. 6a and 6b). All elements have the same size (*0.125x0.125*). The simple *4*-node quadrilateral *FEM* shape functions are taken as partition-of-unity function. All non-enriched covers use the lowest order ($p=1$) polynomial-types cover functions having only

one term ($m=1$). Note that the lowest order ($m^e=1$) enriched-cover-function is identical to the lowest order ($p=1, m=1$) polynomial-types cover function ($\psi_1=1$).

In all the numerical evaluations, two types of relative error norms are computed. The first is L_2 norm, η_2, which is defined as:

$$\eta_2 = \frac{\left\| u^{ex} - u^h \right\|_{L_2}}{\left\| u^{ex} \right\|_{L_2}} \times 100\,\%\,, \qquad \|u\|_{L_2} = \left[\int_\Omega u^2 \, d\Omega \right]^{\frac{1}{2}} \tag{15a-b}$$

The second type is the energy norm, η_e, which is defined as:

$$\eta_e = \frac{\left\| u^{ex} - u^h \right\|_e}{\left\| u^{ex} \right\|_e} \times 100\,\%\,, \qquad \|u\|_e = \left[\int_\Omega (\nabla u \cdot \nabla u)\, d\Omega \right]^{\frac{1}{2}} \tag{15c-d}$$

where $\boldsymbol{u}^{ex}$ and $\boldsymbol{u}^h$ denote respectively the exact and the approximated solution. The rates of convergence of the relative error, $\boldsymbol{R}(\alpha)$, are also computed. It is defined as follows:

$$\boldsymbol{R}(\alpha) = \boldsymbol{log}(\alpha_i/\alpha_{i+1}) \,/\, \boldsymbol{log}(NDOF_{i+1} \,/\, NDOF_i) \tag{16}$$

where $\alpha=\eta_2$ or η_e, $NDOF_{i+1}$ and $NDOF_i$ are the total degrees of freedom in the current and previous case respectively. Tables 1 and 2 show results obtained from single-enrichment scheme while Tables 3 and 4 show results from multi-enrichment scheme. Under the multi-enrichment scheme, Mesh-I has 8 enriched nodal covers, Mesh-II has 21 and Mesh-III has 65. In each case, the total number of degrees of freedom (*NDOF*) is equal to the sum derived from two categories – the enriched and the non-enriched. In the counting, the restrained degrees of freedom along the boundaries are not deducted. For example, Mesh-II under multi-enrichment scheme with $m^e=3$ has *21x3*(=63) degrees of freedom from the enriched covers and *(65-21)x1=44* degrees of freedom from the remaining non-enriched ($p=1, m=1$). The total (*NDOF*) is equal to *63+44=107*. For easy visualization, results of the error norms (η_2 and η_e) against total degrees of freedom are plotted in Figs.7 and 8 respectively. It can be seen that employment of enriched nodal covers with $m^e>1$, (be it single or multi-enrichment

scheme), always leads to more accurate solutions. Obviously, multi-enrichment scheme appears to be superior, particularly when measuring in terms of the energy norm. It is worth noting that under the single-enrichment scheme, results obtained from the two higher-term enrichments ($m^e=3$ and $m^e=4$) are identical. It is because the *3*-term enrichment functions ($m^e=3$) are in fact has the same order of accuracy of the exact solution (Eq.13a). Therefore, *4*-term enrichment function ($m^e=4$) virtually cannot yield better results.

On the other hand, the effect of mesh distortion is investigated through a *21*-node model (see Fig.9) using the multi-enrichment scheme and *4*-term enrichment functions. The total degrees of freedom (*NDOF*) is equal to *(8x4)+(13x1)=45*. The two relative error norms are found to be very small: $\eta_2=0.39\%$ in L_2-norm and $\eta_e=5.10\%$ in energy norm. It demonstrates its insensitiveness to distorted element shape.

3.2

Example2: Motz equation defined over a rectangular domain

In the second example, the problem is governed by the Motz equation, which is defined over the rectangular domain [*-1,1*]×[*0,1*] (see Fig.10). In mathematical form,

$$\begin{cases} -\Delta u = 0 & \text{on } \Omega \\ u = \begin{cases} 500 & \text{on } \Gamma_4 \\ 0 & \text{on } \Gamma_2 \end{cases} \\ \dfrac{\partial u}{\partial n} = 0 & \text{on } \Gamma_1 \cup \Gamma_3 \cup \Gamma_5 \end{cases} \tag{17}$$

The exact solution is [21]:

$$\boldsymbol{u}_{ex} = \sum_{n=0}^{\infty} b_n r^{n+\frac{1}{2}} \cos\left((n+\frac{1}{2})\theta \right) \tag{18a}$$

where $b_0=401.162$; $b_1=87.656$; $b_2=17.238$; $b_3=-8.071$;

$b_4=1.440$; $b_5=0.331$; $b_6=0.275$; ... (18b)

Hence, the asymptotic influence functions may adopt the following forms:

$$\psi_{i1} = 1, \quad \psi_{i2} = r^{1/2}\cos(\frac{\theta}{2}), \quad \psi_{i3} = r^{3/2}\cos(\frac{3\theta}{2}), \quad \psi_{i4} = r^{5/2}\cos(\frac{5\theta}{2}) \tag{19a-d}$$

$$\psi_{i5} = r^{7/2}\cos(\frac{7\theta}{2}), \quad \psi_{i6} = r^{9/2}\cos(\frac{9\theta}{2}), \quad \psi_{i7} = r^{11/2}\cos(\frac{11\theta}{2}) \tag{19e-g}$$

Very often, it is used as a benchmark against a newly developed numerical scheme. Firstly, the performance of single-enrichment scheme versus no-enrichment scheme is investigated. An *8*-element undistorted mesh having *15* nodes (see Fig.11a) is employed. Under the no-enrichment scheme, all nodal cover functions are of polynomial type. Under the single-enrichment scheme, only the cover function for the singular node *A* is enriched. Various results are obtained through *p*-refinements using two to seven terms (m^e*=2~7*) of enriched functions for the single enriched cover. In all cases, the polynomial-typed cover functions are employed for the remaining non-enriched covers. Evaluations of cases go through the lowest order (*p=1*) up to the 5th order (*p=5*). The relative error norms (L_2- and energy-norm) and their rates of convergence are computed. Tables 5 and 6 show the two-, five- and seven-term results (m^e*=2, 5, 7*) for L_2- and energy-norm respectively. They are compared with those obtained under the no-enrichment scheme. For easy visualization, results of the error norms (η_2 and η_e) against total degrees of freedom (*NDOF*) are plotted in Figs.15 and 16 respectively. In the counting of *NDOF*, the restrained degrees of freedom along the boundaries are not deducted. It can be seen that employment of higher-order polynomial-typed cover functions yield more accurate results and exhibit faster rates of convergence. In addition, employment of the *p*-type refinements simultaneously for the enriched and non-enriched covers always leads to improvement of convergence rate.

Subsequently, the performance of multi-enrichment scheme versus single- and no-enrichment schemes is investigated. Under the multi-enrichment scheme, a cluster of nodal covers (including the node *A*'s) is enriched (see Figs. 11b, 12b, 13b and 14b). It results in an enlarged enriched domain covering at least a quarter of the whole problem domain. Under the

single-enrichment scheme, only the cover function for the singular node *A* is enriched (see Figs. 11a, 12a, 13a and 14a). The enriched domain is a small region surrounding the singular node *A*. In all cases, seven-term ($m^e=7$) enriched functions are used for all enriched covers, and the lowest order polynomial-typed cover function ($p=1,m=1$) are used for all other non-enriched covers. The effects of *h*-refinements are also investigated through employment of 4 different meshes. Mesh-I has *15* nodes and *8* elements (see Fig.11). All elements have the same size (*0.5x0.5*). Mesh-II has *45* nodes and *32* elements (see Fig.12). All elements have the same size (*0.25x0.25*). Mesh-III has *153* nodes and *128* elements (see Fig.13). All elements have the same size (*0.125x0.125*). Mesh-IV has *561* nodes and 5*12* elements (see Fig.14). All elements have the same size (*0.0625x0.0625*). Results of the L_2- and energy-norm are shown in Tables 7 and 8 respectively. For easy visualization, they are plotted against the total degrees of freedom (*NDOF*) in Figs.17 and 18 respectively. Obviously, the multi-enrichment schemes yield more accurate results than the single-enrichment schemes do. However, no significant improvements are observed through mesh refinements in both schemes.

On the other hand, the effect of mesh distortion is investigated through a *21*-node model (see Fig.19). Single-enrichment scheme is employed and 7-term enriched functions ($m^e=7$) are used, while all non-enriched cover functions are kept to the lowest order ($p=1, m=1$). The two relative errors are found to be insignificant: $\eta_2=2.44\%$ in L_2-norm and $\eta_e=18.53\%$ in energy norm. It demonstrates its insensitiveness to distorted element shape.

3.3

Example 3: Helmholtz equation in *2D* with singularity

In this example, the problem is governed by the 2D Helmholtz equation, which is defined over the rectangular domain $[-1,1]\times[0,1]$ (see Fig.20). In mathematical form,

$$\begin{cases} -\Delta u + u = 0 & on \ \ \Omega \\ u = \begin{cases} \dfrac{sinh\ (r)}{\sqrt{r}} cos\left(\dfrac{\theta}{2}\right) & on \ \ \Gamma_1, \Gamma_4, \Gamma_5 \\ 0 & on \ \ \Gamma_2 \end{cases} \\ \dfrac{\partial u}{\partial n} = 0 & on \ \ \Gamma_3 \end{cases} \tag{20}$$

There exists strong singularity in the vicinity of the singular point *A at* (*0,0*) and the exact solution is [21]:

$$\boldsymbol{u}_{ex}(r, \theta) = \frac{sinh\ (r)}{\sqrt{r}} cos\left(\frac{\theta}{2}\right) \tag{21}$$

Hence, the asymptotic influence functions may adopt the following forms:

$$\boldsymbol{\psi}_{i1} = 1, \quad \boldsymbol{\psi}_{i2} = r^{-1/2} sinh(r)\ cos(\frac{\theta}{2}) \tag{22a-b}$$

Note that in this *2D* Helmholtz problem, the solution itself is singular (of order $r^{-1/2}$). Hence, it is a more difficult problem in comparison with the two previous problems, in which only the derivatives of the solution are singular.

Firstly, the performance of single-enrichment scheme versus no-enrichment scheme is investigated. The same *8*-element undistorted mesh having *15* nodes used in Example 2 (see Fig.11a) is employed. Under the no-enrichment scheme, all nodal cover functions are of the polynomial type. Under the single-enrichment scheme, only the cover function for the singular node *A* is enriched with two terms ($m^e=2$). In all cases, the polynomial-typed cover functions are employed for the remaining non-enriched covers. Evaluations of cases go through the lowest order ($p=1$) up to the 5th order ($p=5$). The relative error norms (L_2- and energy-norm) and their rates of convergence are computed and shown in Tables 9 and 10 respectively. For easy visualization, results of the error norms (η_2 and η_e) against total degrees of freedom (*NDOF*) are plotted in Figs.21 and 22 respectively. Note that the relative error in energy norm, η_e, is defined as follows:

$$\eta_e = \frac{\left\| u^{ex} - u^{h} \right\|_e}{\left\| u^{ex} \right\|_e} \times 100\ \% \ , \qquad \|u\|_e = [\int_{\Omega} (\nabla u \cdot \nabla u + u \cdot u) d\Omega]^{\frac{1}{2}} \qquad (23a\text{-}b)$$

From Figs. 21 and 22 and Tables 9 and 10, it can be seen that merely employment of the single-enrichment scheme with two-term enriched function can yield much more accurate results. On the other hand, it also reveals that the single-enrichment scheme going with higher-order polynomial functions for the non-enriched covers does not lead to much improvement of the convergence rate.

Subsequently, the performance of multi-enrichment scheme versus single- and no-enrichment schemes is investigated. Under the multi-enrichment scheme, a cluster of nodal covers (including the node *A*'s) is enriched (see Figs. 11b, 12b, 13b and 14b). It results in an enlarged enriched domain covering at least a quarter of the whole problem domain. Under the single-enrichment scheme, only the cover function for the singular node *A* is enriched (see Figs. 11a, 12a, 13a and 14a). The enriched domain is a small region surrounding the singular node *A*. In all cases, two-term ($m^e=2$) enriched functions are used for all enriched covers, and the lowest order polynomial-typed cover function ($p=1,m=1$) are used for all other non-enriched covers. The effects of *h*-refinements are also investigated through employment of 4 different meshes same as those used in Example 2. Results of the L_2- and energy-norm are shown in Tables 11 and 12 respectively. For easy visualization, they are plotted against the total degrees of freedom (*NDOF*) in Figs.23 and 24 respectively. Once again, the results show that the multi-enrichment schemes yield more accurate solutions than the single-enrichment schemes do. However, both schemes show only little improvement in convergence rates through the *h*-refinements.

Finally, the sensitiveness to distorted mesh is investigated. The same *21*-node distorted mesh as in Example 2 is used (see Fig.19). Single-enrichment scheme is employed and 2-term enriched functions ($m^e=2$) are used, while all non-enriched cover functions are kept to the

lowest order ($p=1, m=1$). The two relative errors are found to be insignificant: $\eta_2=2.5\%$ in L_2-norm and $\eta_e=13.0\%$ in energy norm. It demonstrates again its insensitiveness to distorted element shape.

4

Conclusions

Incorporating *prior* analytical information as enriched cover functions in the *PUFEM* procedures is demonstrated, particularly for solving singular boundary-value problems. Multi-nodal-enrichment and single nodal-enrichment schemes are illustrated. The performance and effect of *p*-type and *h*-type refinements in both schemes are investigated. The accuracy is judged from the relative error norms. Results show that multi-enrichment schemes always yield more accurate results than the single-enrichment schemes, which in turn perform better than the no-enrichment schemes do. Be it under single or multi-enrichment scheme, employment of more enrichment terms often leads to more accurate solution. Another measure of the performance is the rate of convergence. Under the multi-enrichment scheme, the *p*-type refinements often lead to remarkable improvement in convergence rate, while the *h*-type exhibits little improvement. Under the single-enrichment scheme, it exhibits improvements in some cases either through *p*-type or *h*-type refinements, but the improvements are not guaranteed. In all, employment of the *p*-type refinements simultaneously, for both the enriched covers and the non-enriched covers, always leads to improvement of convergence rate measured in terms of energy norm. Moreover, the *PUFEM* procedure is found to be insensitive to the element-mesh distortion. The examples demonstrate the robustness of the *PUFEM* in solving singular boundary-value problems.

References

1. **Lucy L B** (1977) A numerical approach to the testing of the fission hypothesis. Astron. J. 8(12): 1013-1024
2. **Nayroles B, Touzot G, Villon P** (1992) Generalizing the finite element method: Diffuse approximation and diffuse elements. Comput. Mech. 10: 307-318
3. **Belytschko T., Gu L. and Lu Y. Y.** (1994) Fracture and Crack Growth by Element Free Galerkin Methods. Modeling Simul. Material Science Engrg. 2: 519-534
4. **Belytschko T, Krongauz Y, Organ D, Fleming M, Krysl P** (1996) Meshless methods - An overview and recent developments. Comput. Methods Appl. Mech. Engrg. 139: 3-47
5. **Liu W K, Chen Y, Chang C T, Belytschko T** (1996) Advances in multiple scale kernel particle methods. Comput. Mech. 18: 73-111
6. **Duarte C A, Oden J T** (1996) Hp-Clouds - An h-p meshless method. Numer. Methods for Partial Differential Equations 12: 673-705
7. **Oden J T, Duarte C A, Zienkiewicz O C** (1998) A new cloud-based hp finite element method. Int. J. Numer. Methods Engrg. 50: 160-170
8. **Babuska I, Melenk J M** (1997) The partition of unity method. Int. J. Numer. Methods Engrg. 40: 727-758
9. **Melenk J M, Babuska I** (1996) The partition of unity finite element method: basic theory and application. Comput. Methods Appl. Mech. Engrg. 139: 289-314
10. **Strouboulis T, Babuska I, Copps K** (2000) The design and analysis of the generalized finite element method. Comput. Methods Appl. Mech. Engrg. 181: 43-69
11. **Onate E, Idelsohn S, Zienkiewicz O C, Taylor R L** (1996) A finite point method in computational mechanics - Applications to convective transport and fluid flow. Int. J. Numer. Methods Engrg. 39: 3839-3866

12. **Shi G-H** (1995) Working forum on the manifold method of material analysis - organized by Geotechnical Laboratory, US Army Corps of Engineers, Waterways Experiment Station 1-232
13. **Braun J, Sambridge M** (1995) A numerical method for solving partial differential equations on highly irregular evolving grids. Nature 376: 655-660
14. **Atluri S N, Zhu T** (1998) A new meshless local Petrov-Galerkin (MLPG) approach in computational mechanics. Comput. Mech. 22:117-127
15. **Sheng N, Fan S C** (1999) Meshless finite element method to solve boundary-value problems. Proc. 4th Asian-Pacific Conference on Computational Mechanics, Singapore, 2: 961-966
16. **Zhang X, Liu X, Lu M-W, Chen Y** (2001) Imposition of essential boundary conditions by displacement constraint equations in meshless methods. Commun. Numer. Meth. Engng. 17:165-178
17. **Zienkiewicz O C, Zhu J Z, Gong N G** (1989) Effective and practical h-p-version adaptive analysis procedures for the finite element method, Int. J. Numer. Methods Engrg. 28: 879-891
18. **Lee C K, Hobbs R E** (1997) Automatic adaptive refinements for shell analysis using nine-node assumed strain element. Int. J. Numer. Methods Engrg. 40: 3601-3638
19. **Yosibash Z, Szabo B** (1995) Numerical analysis of singularities in two-dimension - Part 1: computation of eigenpairs. Int. J. Numer. Methods Engrg. 38: 2055-2082
20. **Oh H S, Babuska I** (1995) The method of auxiliary mapping for the finite element solutions of elasticity problems containing singularities. J. Comput. Phy. 121, 193-212
21. **Yosibash Z, Schiff B** (1997) A super-element for the finite element solution of two-dimensional elliptic problems with boundary singularities. Fin. Ele. Anal. Design 26: 315-335

22. **Belytschko T, Black T** (1999) Elastic crack growth in finite elements with minimal remeshing. Int. J. Numer. Methods Engrg. 45(5): 601-620
23. **Babuska I, Anderson B, Guo B** (1996) Finite element method for solving problems with singular solutions, J. Comput. Appl. Math. 74(1-2): 51-70
24. **Fan S C, Luah M H** (1990) A new spline finite element for the analysis of shells of revolution. J. Engng. Mech. ASCE 116(3): 709-726

Table 1. Relative error in L_2 norm and rate of convergence for Example 1 under single-enrichment scheme

Mesh	Terms of enriched functions employed											
	1-term (m^e=1)			2-term (m^e=2)			3-term (m^e=3)			4-term (m^e=4)		
	NDOF	η_2	$R(\eta_2)$	*NDOF*	η_2	$R(\eta_2)$	*NDOF*	η_2	$R(\eta_2)$	*NDOF*	η_2	$R(\eta_2)$
I	21	1.02	—	22	0.42	—	23	0.40	—	24	0.40	—
II	65	0.43	0.77	66	0.24	0.51	67	0.24	0.49	68	0.24	0.49
III	225	0.25	0.44	226	0.21	0.11	227	0.21	0.10	228	0.21	0.10

Note: all non-enriched cover functions are of the lowest order (*p=1, m=1*)

Table 2. Relative error in energy norm and rate of convergence for Example 1 under single-enrichment scheme

Mesh	Terms of enriched functions employed											
	1-term (m^e=1)			2-term (m^e=2)			3-term (m^e=3)			4-term (m^e=4)		
	NDOF	η_e	$R(\eta_e)$	*NDOF*	η_e	$R(\eta_e)$	*NDOF*	η_e	$R(\eta_e)$	*NDOF*	η_e	$R(\eta_e)$
I	21	13.4	—	22	8.20	—	23	7.84	—	24	7.84	—
II	65	8.65	0.39	66	5.45	0.37	67	5.37	0.35	68	5.37	0.36
III	225	5.64	0.34	226	3.81	0.29	227	3.79	0.29	228	3.79	0.29

Note: all non-enriched cover functions are of the lowest order (*p=1, m=1*)

Table 3. Relative error in L_2 norm and rate of convergence for Example 1 under multi-enrichment scheme

Mesh	Terms of enriched functions employed											
	1-term (m^e=1)			2-term (m^e=2)			3-term (m^e=3)			4-term (m^e=4)		
	NDOF	η_2	$R(\eta_2)$	*NDOF*	η_2	$R(\eta_2)$	*NDOF*	η_2	$R(\eta_2)$	*NDOF*	η_2	$R(\eta_2)$
I	21	1.02	—	29	0.42	—	37	0.36	—	45	0.32	—
II	65	0.43	0.77	86	0.23	0.55	107	0.23	0.42	128	0.22	0.36
III	225	0.25	0.44	290	0.21	0.08	355	0.21	0.08	420	0.21	0.04

Note: all non-enriched cover functions are of the lowest order (*p=1, m=1*)

Table 4. Relative error in energy norm and rate of convergence for Example 1 under multi-enrichment scheme

Mesh	Terms of enriched functions employed											
	1-term (m^e=1)			2-term (m^e=2)			3-term (m^e=3)			4-term (m^e=4)		
	NDOF	η_e	$R(\eta_e)$	*NDOF*	η_e	$R(\eta_e)$	*NDOF*	η_e	$R(\eta_e)$	*NDOF*	η_e	$R(\eta_e)$
I	21	13.4	—	29	6.96	—	37	5.91	—	45	5.37	—
II	65	8.65	0.39	86	4.45	0.41	107	4.04	0.36	128	3.57	0.39
III	225	5.64	0.34	290	3.05	0.31	355	2.86	0.29	420	2.56	0.28

Note: all non-enriched cover functions are of the lowest order (*p=1, m=1*)

Table 5. Relative error in L_2 norm and rate of convergence for Example 2 under single-enrichment scheme

Non-enriched functions		Terms of enriched functions employed											
		Without enrichment			2-term (m^e=2)			5-term (m^e=5)			7-term (m^e=7)		
Order *p*	Term *m*	*NDOF*	η_2	$R(\eta_2)$	*NDOF*	η_2	$R(\eta_2)$	*NDOF*	η_2	$R(\eta_2)$	*NDOF*	η_2	$R(\eta_2)$
1	1	15	6.37	—	16	1.47	—	19	1.47	—	21	1.44	—
2	3	45	4.38	0.34	44	0.96	0.42	47	0.92	0.52	49	0.91	0.54
3	7	105	2.47	0.68	100	0.50	0.80	103	0.40	1.06	105	0.35	1.25
4	12	180	1.40	1.05	170	0.34	0.73	173	0.17	1.65	175	0.16	1.53
5	18	270	1.07	0.66	254	0.27	0.57	257	0.09	1.61	259	0.08	1.77

Table 6. Relative error in energy norm and rate of convergence for Example 2 under single-enrichment scheme

Non-enriched functions		Terms of enriched functions employed											
		Without enrichment			2-term (m^e=2)			5-term (m^e=5)			7-term (m^e=7)		
Order *p*	Term *m*	*NDOF*	η_e	$R(\eta_e)$	*NDOF*	η_e	$R(\eta_e)$	*NDOF*	η_e	$R(\eta_e)$	*NDOF*	η_e	$R(\eta_e)$
1	1	15	28.0	—	16	14.4	—	19	13.9	—	21	14.0	—
2	3	45	23.0	0.18	44	8.98	0.47	47	8.78	0.51	49	8.98	0.52
3	7	105	16.6	0.39	100	5.74	0.55	103	5.07	0.70	105	4.77	0.83
4	12	180	12.4	0.54	170	4.97	0.27	173	2.78	1.16	175	2.62	1.17
5	18	270	11.0	0.30	254	4.44	0.28	257	1.66	1.30	259	1.56	1.32

Table 7. Relative error in L_2 norm and rate of convergence for Example 2 under various enrichment schemes

Mesh	Without enrichment			Single-enrichment (m^e=7)			Multi-enrichment (m^e=7)		
	NDOF	η_2	$R(\eta_2)$	*NDOF*	η_2	$R(\eta_2)$	*NDOF*	η_2	$R(\eta_2)$
I	15	6.37	—	21	1.44	—	51	0.58	—
II	45	2.98	0.69	51	0.61	0.97	135	0.26	0.82
III	153	1.44	0.59	159	0.29	0.66	423	0.095	0.88
IV	561	0.71	0.54	567	0.15	0.52	1479	0.052	0.48

Note: all non-enriched cover functions are of the lowest order (*p=1, m=1*)

Table 8. Relative error in energy norm and rate of convergence for Example 2 under various enrichment schemes

Mesh	Without enrichment			Single-enrichment (m^e=7)			Multi-enrichment (m^e=7)		
	NDOF	η_e	$R(\eta_e)$	*NDOF*	η_e	$R(\eta_e)$	*NDOF*	η_e	$R(\eta_e)$
I	15	28.0	—	21	14.0	—	51	7.42	—
II	45	19.0	0.35	51	9.35	0.45	135	5.13	0.38
III	153	13.6	0.27	159	6.41	0.33	423	2.93	0.49
IV	561	9.53	0.27	567	4.50	0.28	1479	1.67	0.45

Note: all non-enriched cover functions are of the lowest order (*p=1, m=1*)

Table 9. Relative error in L_2 norm and rate of convergence for Example 3 under single-enrichment scheme

Non-enriched functions		Without enrichment			Single-enrichment (m^e=2)		
Order ***p***	**Term** ***m***	***NDOF***	η_2	$R(\eta_2)$	***NDOF***	η_2	$R(\eta_2)$
1	1	15	4.03	—	16	2.09	—
2	3	45	3.27	0.19	46	1.40	0.38
3	7	105	2.16	0.49	106	1.35	0.04
4	12	180	1.62	0.53	181	1.20	0.22
5	18	270	1.30	0.54	271	1.15	0.11

Table 10. Relative error in energy norm and rate of convergence for Example 3 under single-enrichment scheme

Non-enriched functions		Without enrichment			Single-enrichment (m^e=2)		
Order ***p***	**Term** ***m***	***NDOF***	η_e	$R(\eta_e)$	***NDOF***	η_e	$R(\eta_e)$
1	1	15	24.0	—	16	13.4	—
2	3	45	19.7	0.18	46	9.01	0.38
3	7	105	16.5	0.21	106	7.46	0.23
4	12	180	12.9	0.46	181	6.36	0.30
5	18	270	10.5	0.51	271	5.41	0.40

Table 11. Relative error in L_2 norm and rate of convergence for Example 3 under various enrichment schemes

Mesh	Without enrichment			Single-enrichment (m^e=2)			Multi-enrichment (m^e=2)		
	NDOF	η_2	$R(\eta_2)$	*NDOF*	η_2	$R(\eta_2)$	*NDOF*	η_2	$R(\eta_2)$
I	15	4.03	—	16	2.09	—	21	2.16	—
II	45	1.88	0.69	46	0.54	1.28	60	0.58	1.25
III	153	0.91	0.59	154	0.18	0.91	198	0.15	1.13
IV	561	0.45	0.54	562	0.083	0.60	714	0.045	0.94

Note: all non-enriched cover functions are of the lowest order (*p=1, m=1*)

Table 12. Relative error in energy norm and rate of convergence for Example 3 under various enrichment schemes

Mesh	Without enrichment			Single-enrichment (m^e=2)			Multi-enrichment (m^e=2)		
	NDOF	η_e	$R(\eta_e)$	*NDOF*	η_e	$R(\eta_e)$	*NDOF*	η_e	$R(\eta_e)$
I	15	24.0	—	16	13.4	—	21	13.0	—
II	45	16.6	0.34	46	8.21	0.46	60	7.12	0.57
III	153	12.0	0.27	154	5.52	0.33	198	3.87	0.51
IV	561	8.18	0.30	562	3.83	0.28	714	2.09	0.48

Note: all non-enriched cover functions are of the lowest order (*p=1, m=1*)

List of figures:

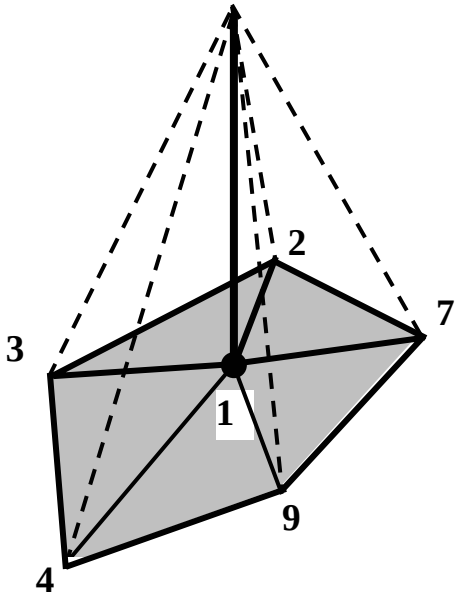

(a)

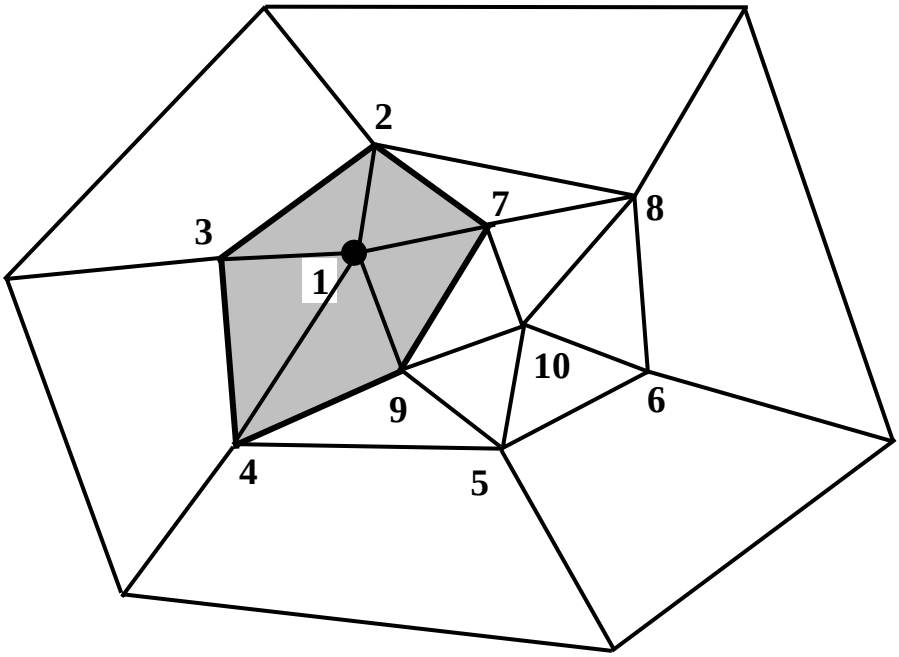

(b)

Fig. 1. : (a) C^0 Partition-of-unity function defined over the domain Ω_1 for node 1; (b) Nodal cover of node 1

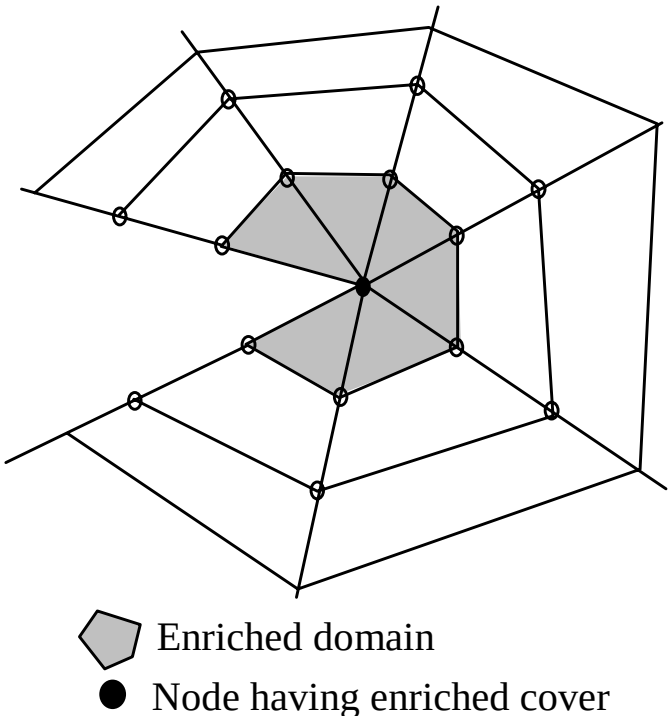

(a)

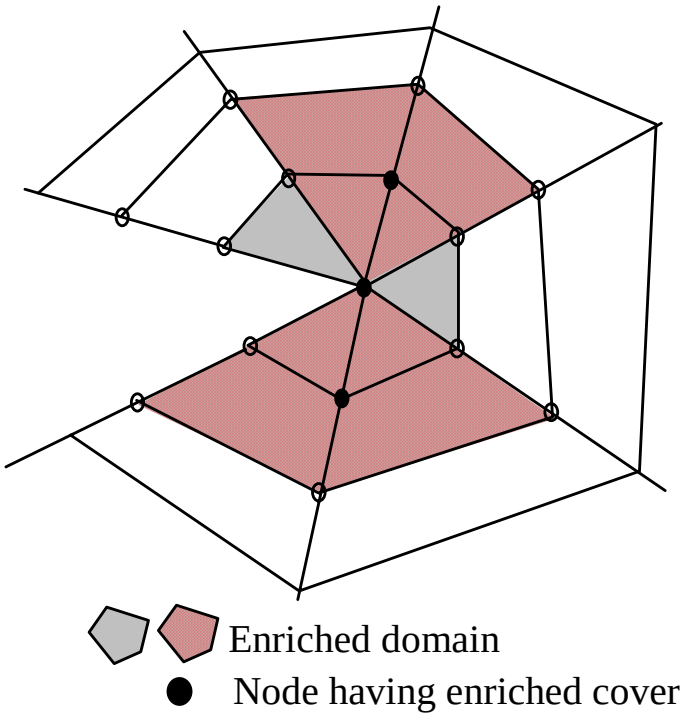

(b)

Fig. 2. (a) Single nodal cover enrichment; (b) Multi-nodal cover enrichment

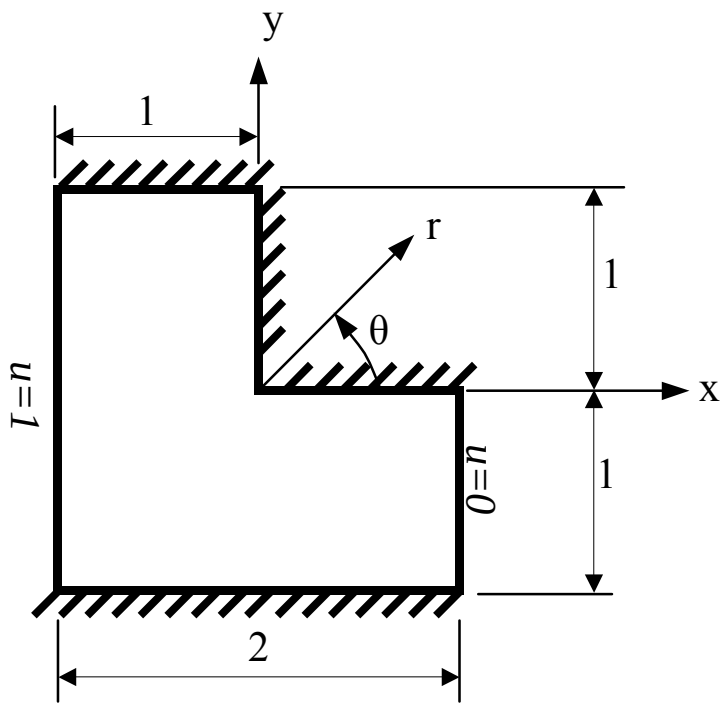

Fig. 3. Domain and boundary conditions (Example 1)

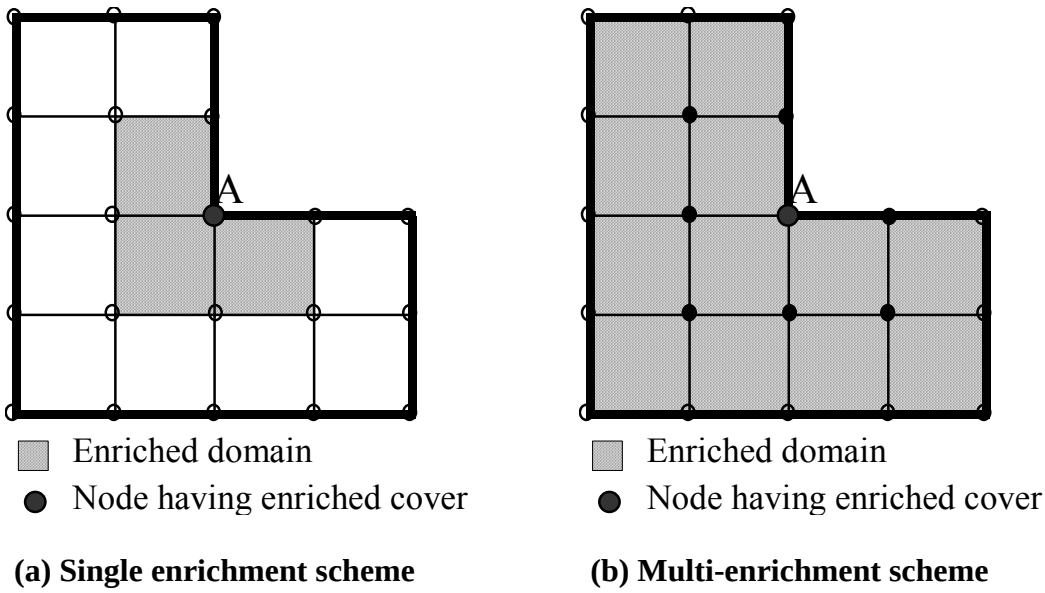

(a) Single enrichment scheme **(b) Multi-enrichment scheme**

Fig. 4. Mesh-I nodal configuration and enrichment schemes (Example 1)

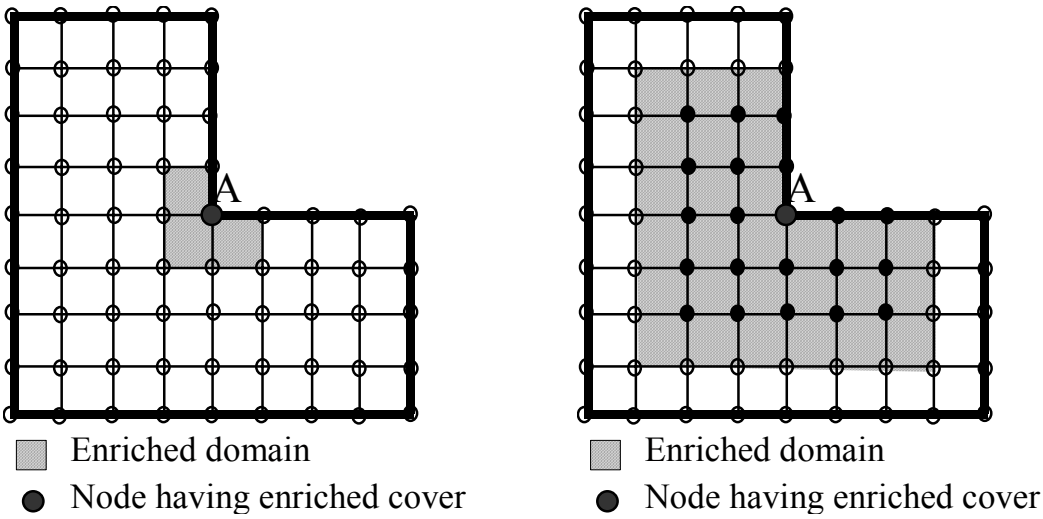

(a) Single enrichment scheme **(b) Multi-enrichment scheme**

Fig. 5. Mesh-II nodal configuration and enrichment schemes (Example 1)

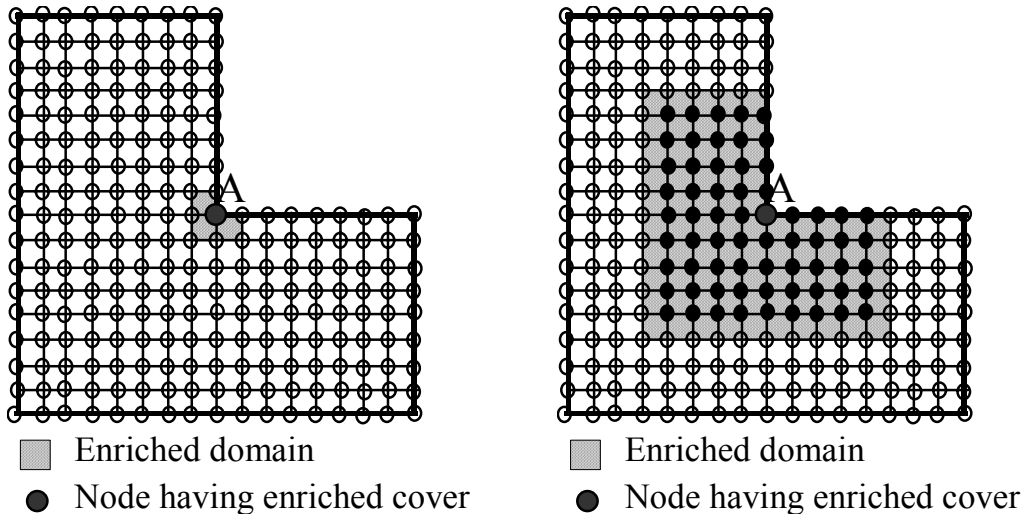

(a) Single enrichment scheme **(b) Multi-enrichment scheme**

Fig. 6. Mesh-III nodal configuration and enrichment schemes (Example 1)

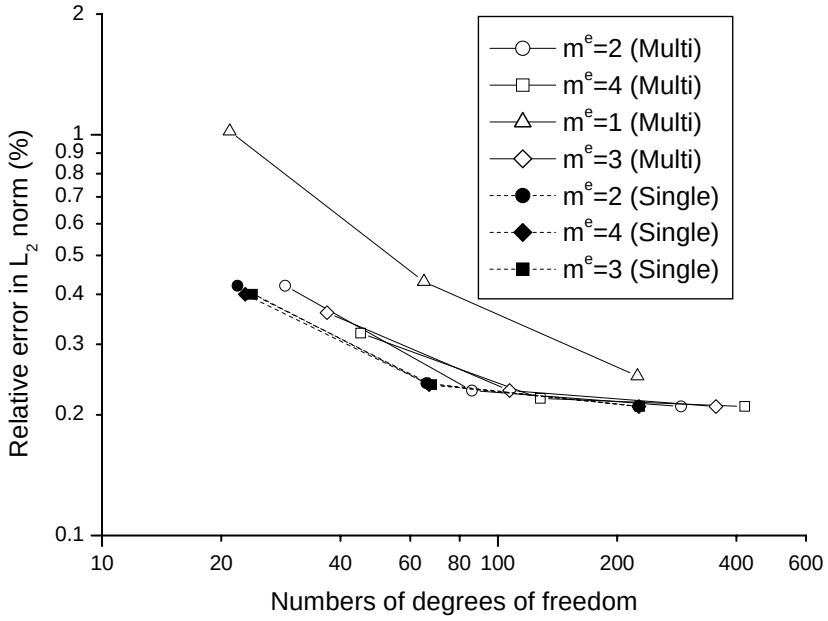

Fig. 7. Relative error in L_2 norm against total DOF (Example 1)

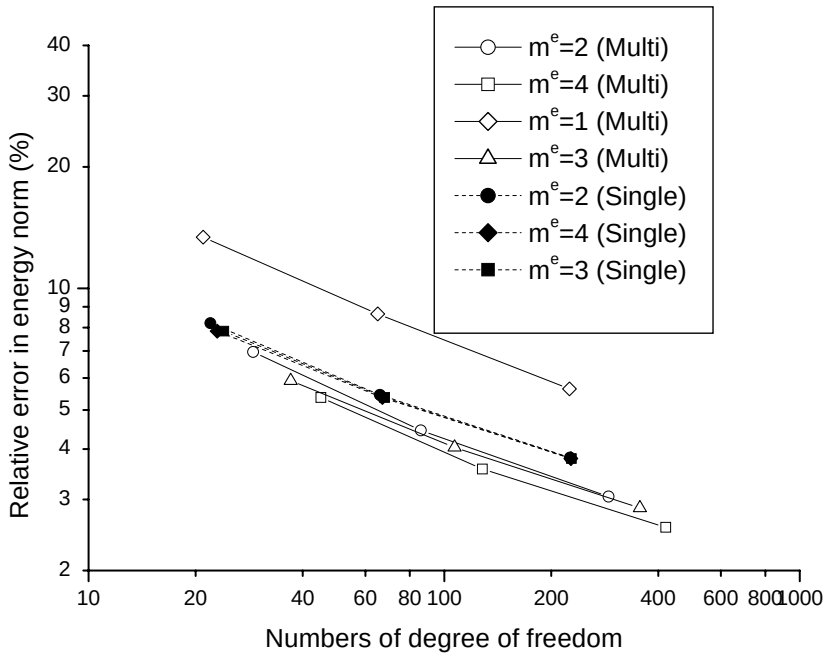

Fig. 8. Relative error in energy norm against total DOF (Example 1)

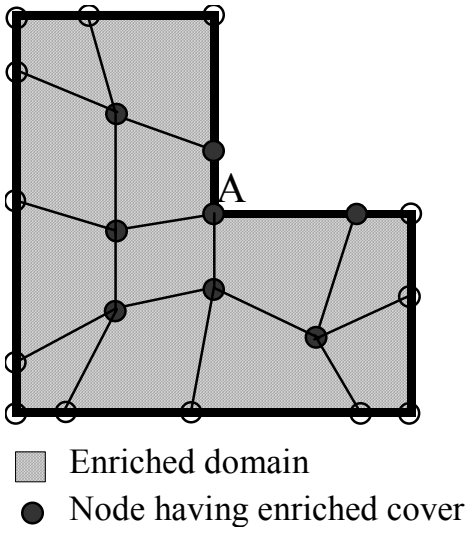

Fig. 9. 21-node distorted mesh configuration (Example 1)

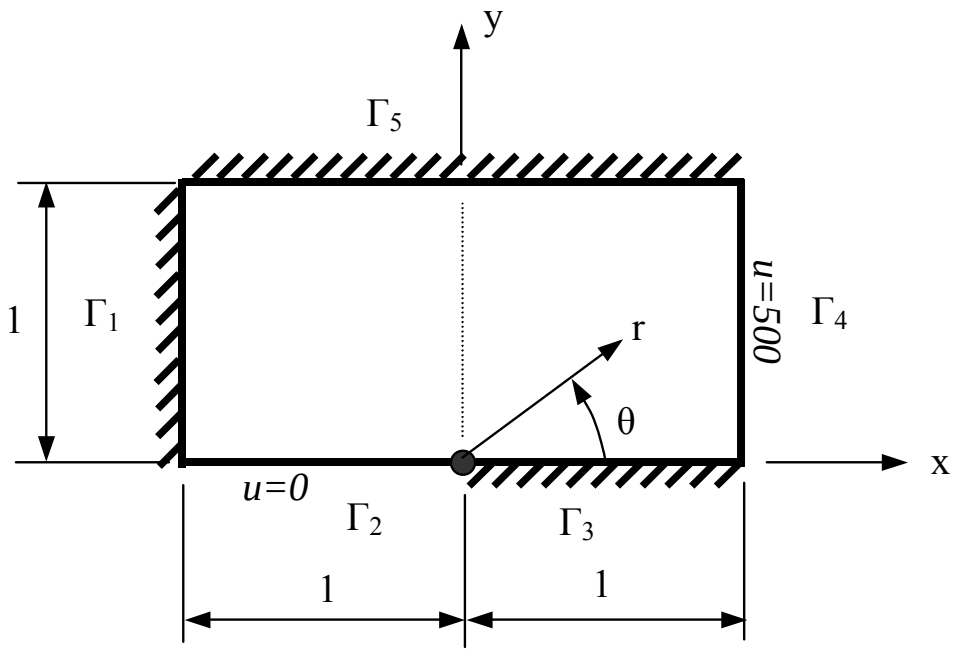

Fig. 10. Domain and boundary conditions (Example 2)

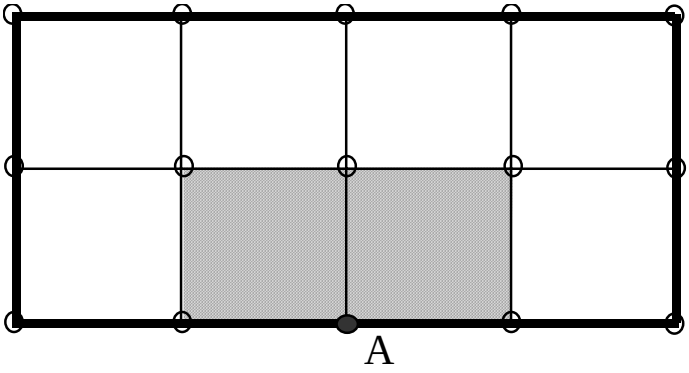

(a) Single enrichment scheme

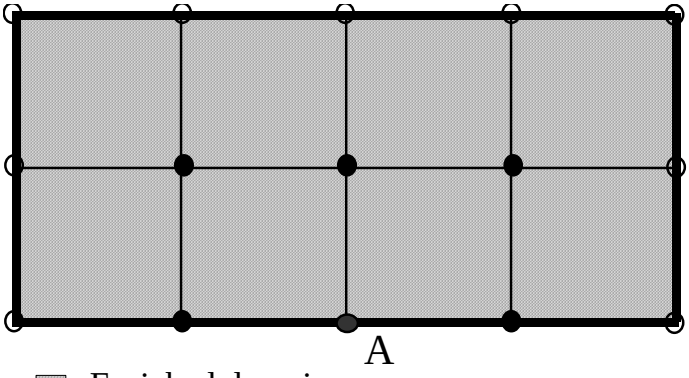

(b) Multi-enrichment scheme

Fig. 11. Mesh-I nodal configuration and enrichment schemes (Examples 2 & 3)

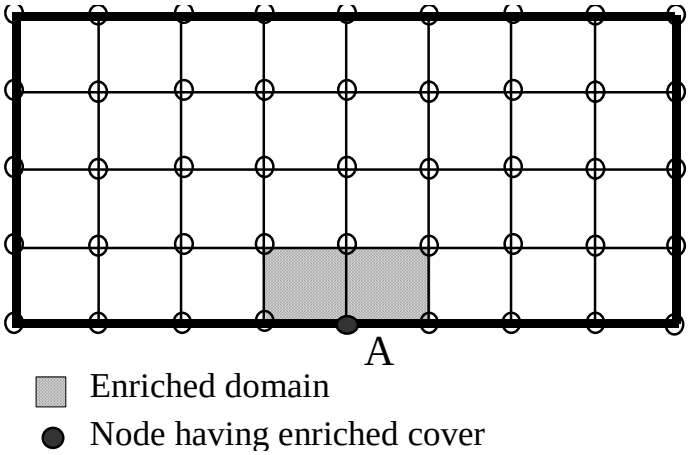

(a) Single enrichment scheme

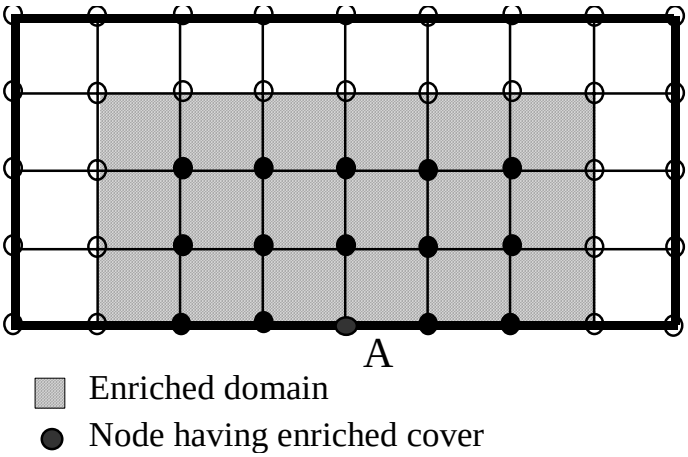

(b) Multi-enrichment scheme

Fig. 12. Mesh-II nodal configuration and enrichment schemes (Examples 2 & 3)

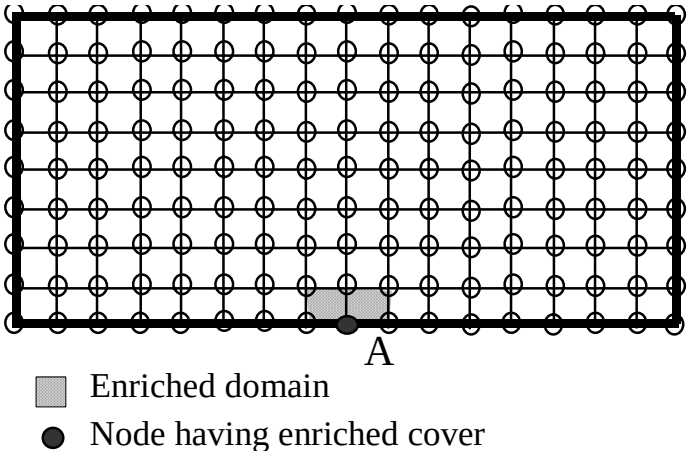

(a) Single enrichment scheme

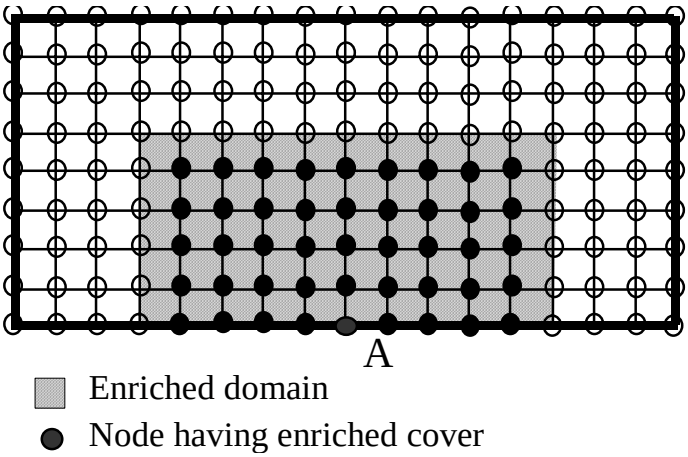

(b) Multi-enrichment scheme

Fig. 13. Mesh-III nodal configuration and enrichment schemes (Examples 2 & 3)

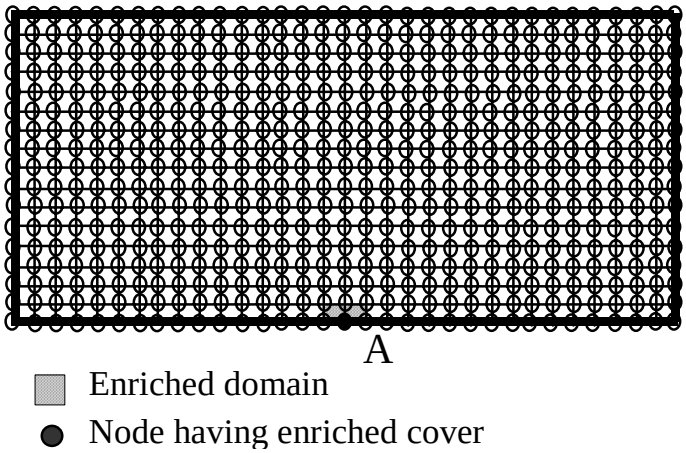

(a) Single enrichment scheme

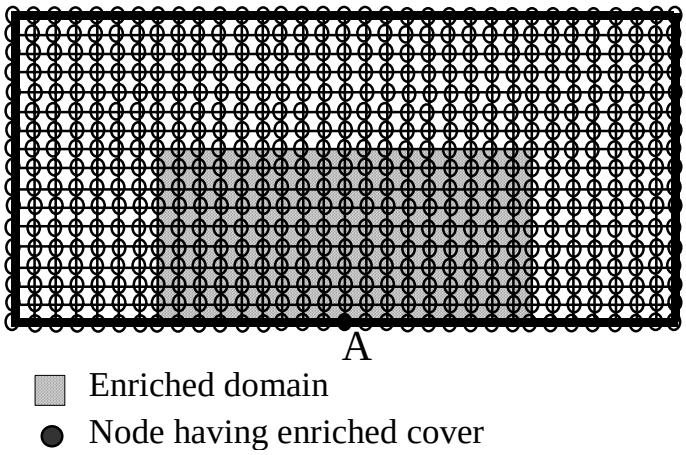

(b) Multi-enrichment scheme

Fig. 14. Mesh-IV nodal configuration and enrichment schemes (Examples 2 & 3)

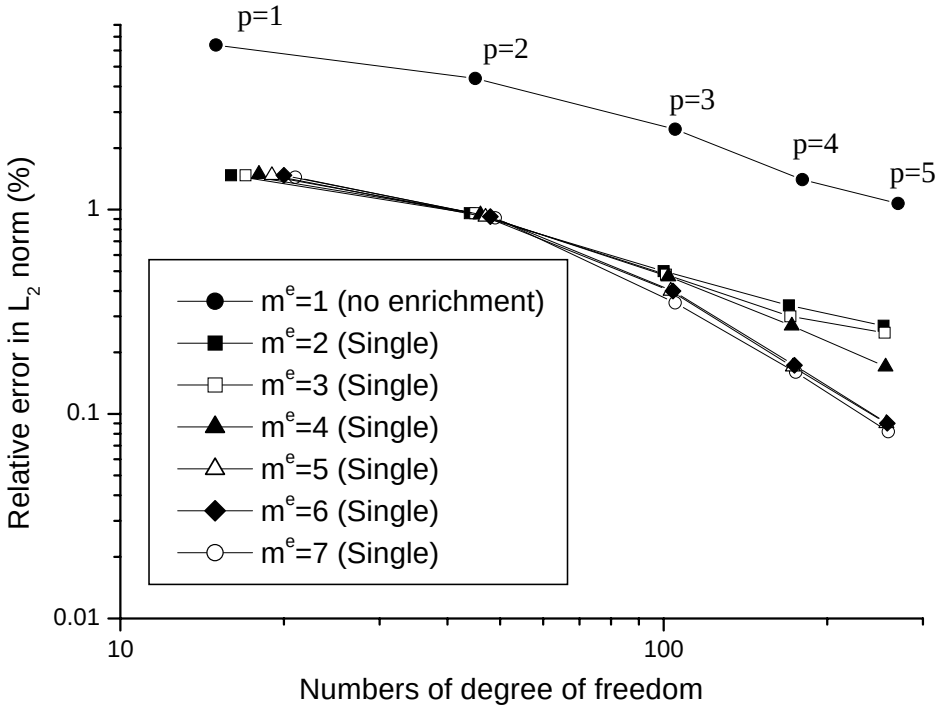

Fig. 15. Relative error in L_2 norm against total DOF (Example 2) –'*p*-refinement'

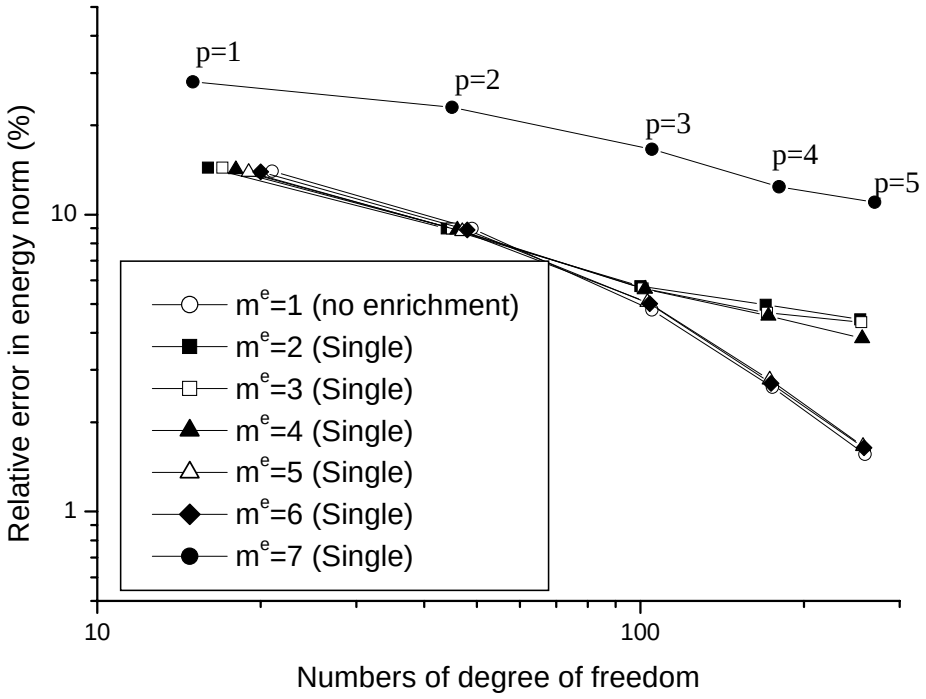

Fig. 16. Relative error in energy norm against total DOF (Example 2) –'*p*-refinement'

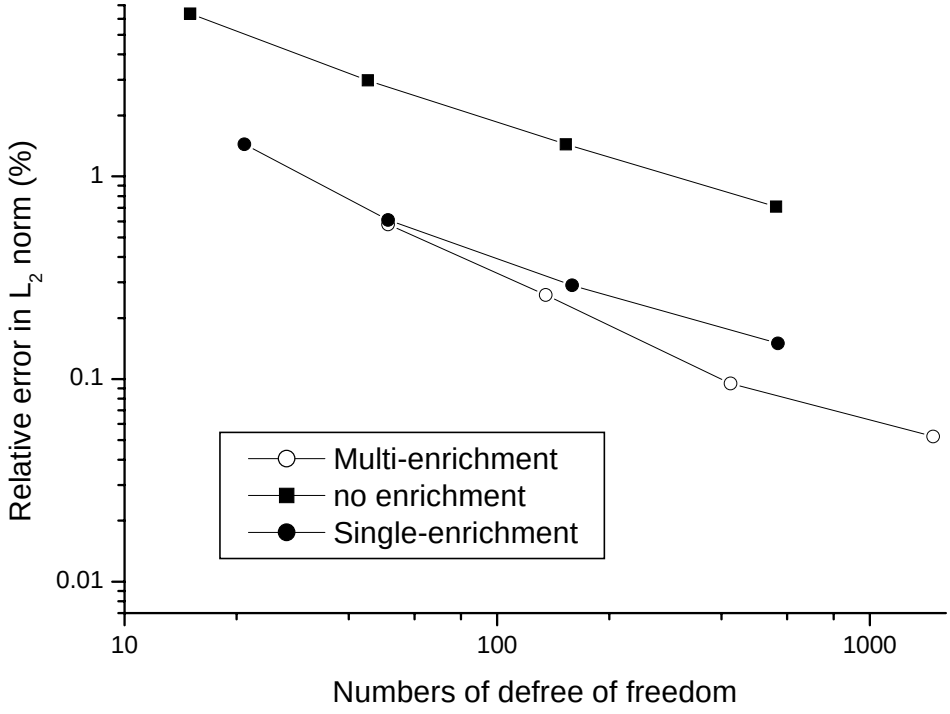

Fig. 17. Relative error in L_2 norm against total DOF (Example 2) –'*h*-refinement'

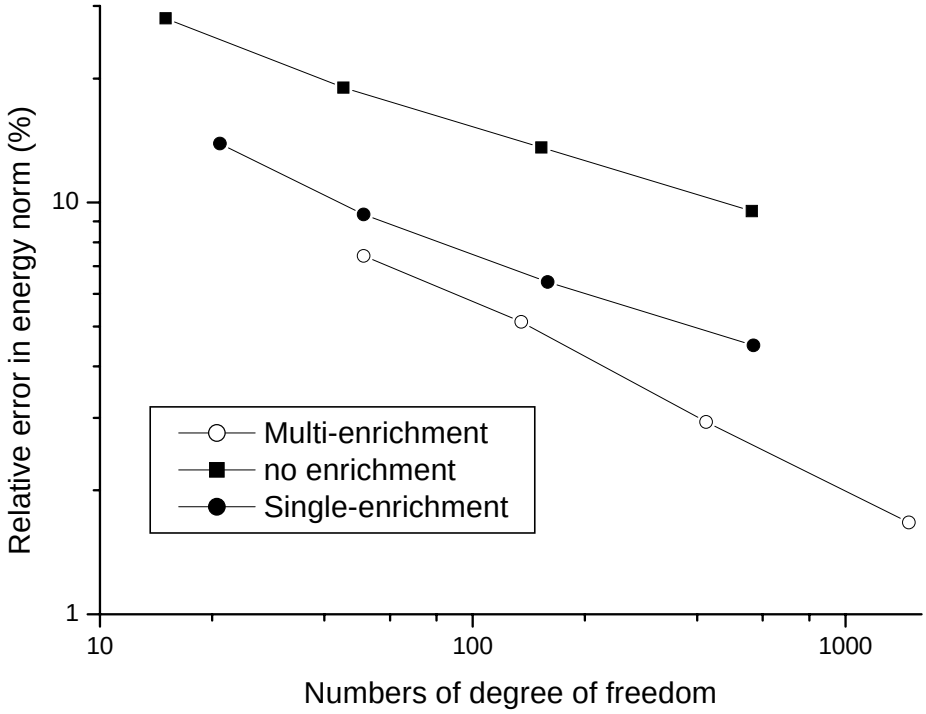

Fig. 18. Relative error in energy norm against total DOF (Example 2) –'*h*-refinement'

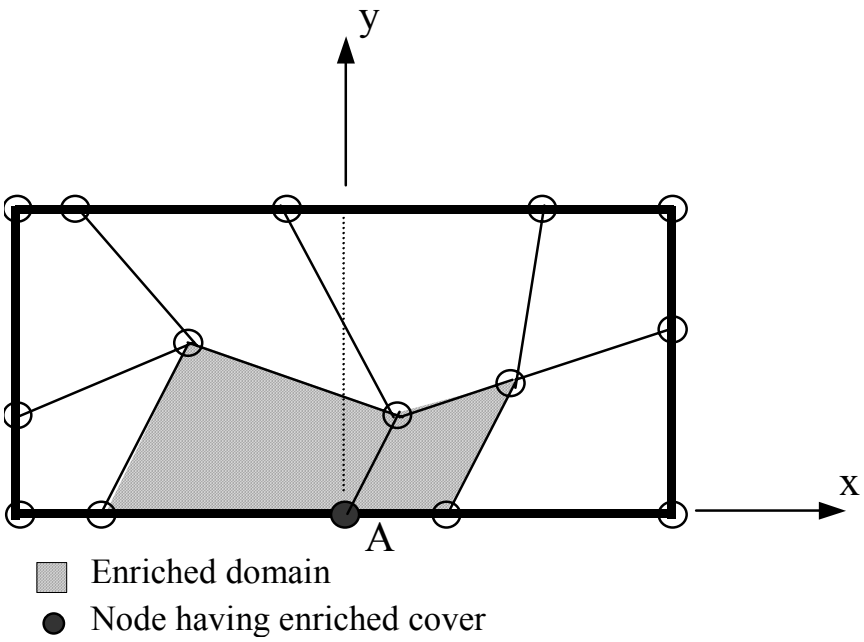

Fig. 19. 15-node distorted mesh configuration (Examples 2 & 3)

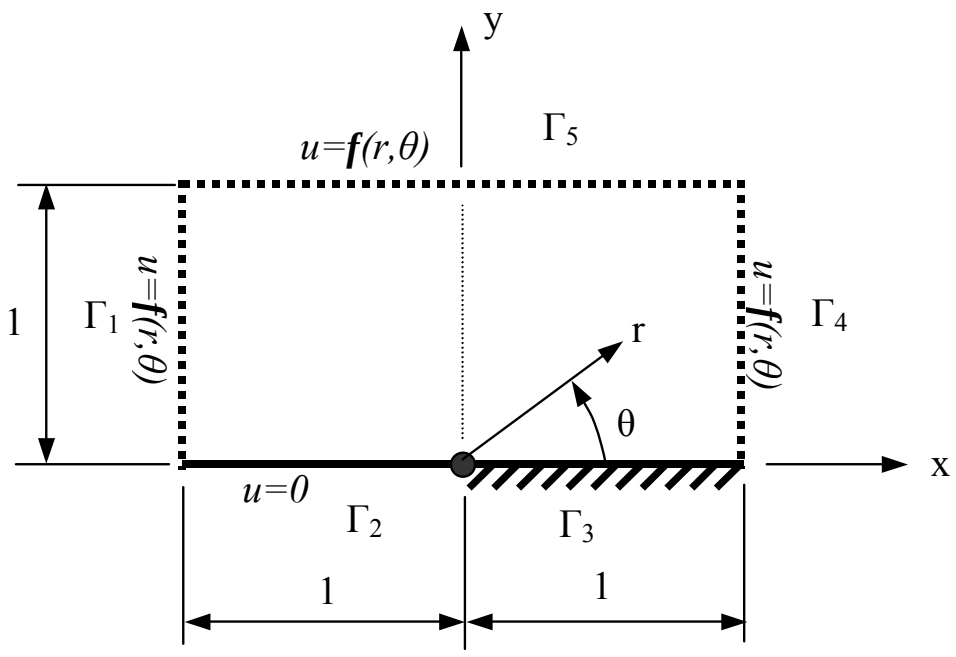

Fig. 20. Domain and boundary conditions (Example 3)

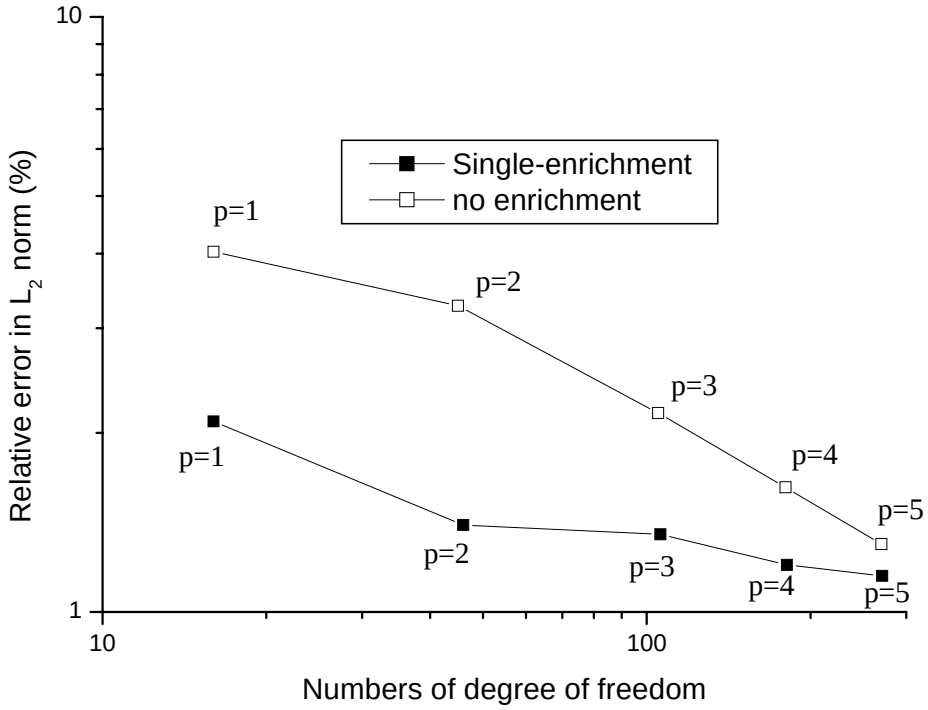

Fig. 21. Relative error in L_2 norm against total DOF (Example 3) –'*p*-refinement'

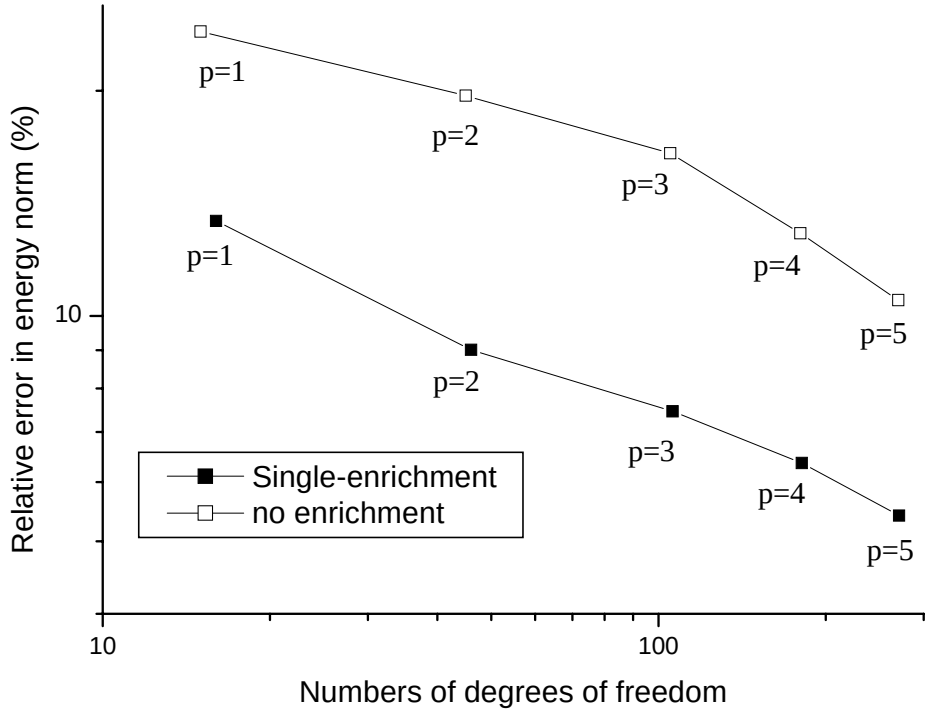

Fig. 22. Relative error in energy norm against total DOF (Example 3) –'*p*-refinement'

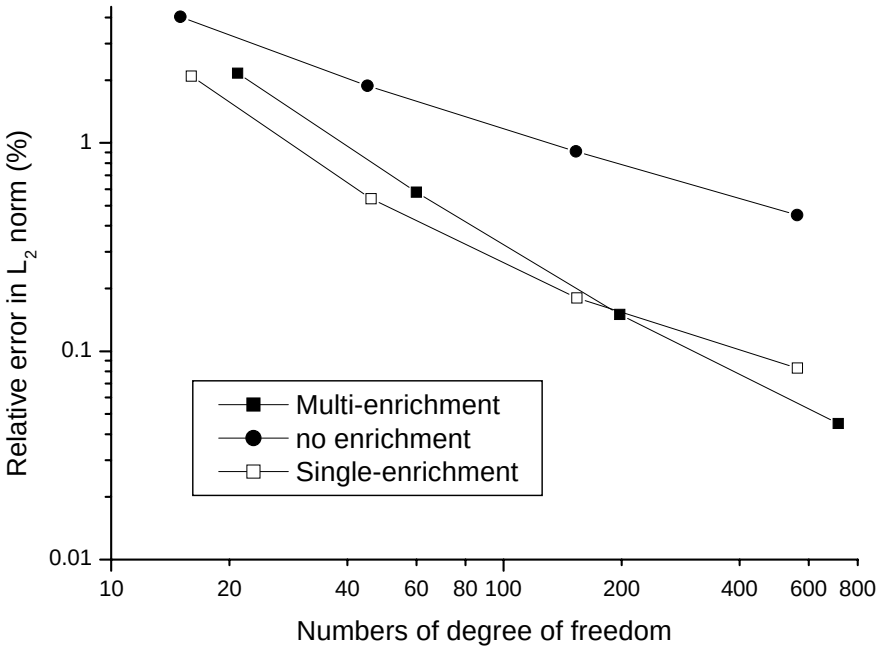

Fig. 23. Relative error in L_2 norm against total DOF (Example 3) - *h*-refinement

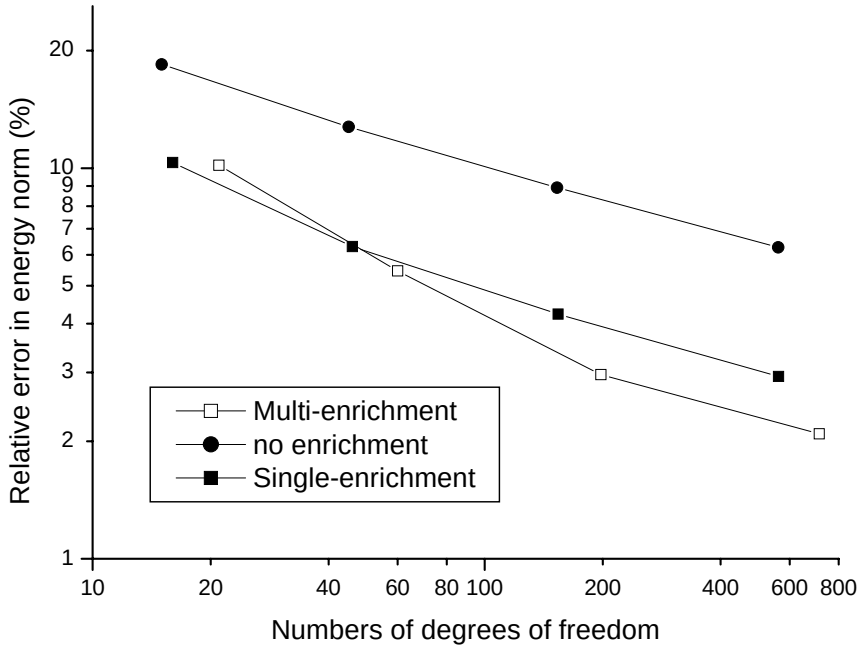

Fig. 24. Relative error in energy norm against total DOF (Example 3) - *h*-refinement